

CHAPTER 38

THE ENERGY BUDGET OF THE URBAN SURFACE: TWO LOCATIONS IN DUBLIN

STEPHANIE KEOGH, GERALD MILLS*, and ROWAN FEALY

Forthcoming in *Irish Geography*.

Introduction

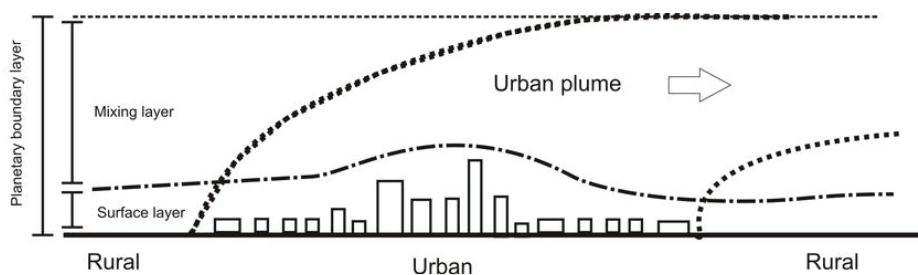
In the first decade of the 21st Century a significant milestone was reached when the urban proportion of the world's population of 6.6 billion passed 50%. This proportion will increase rapidly in the decades to come as parts of Asia and Africa become progressively less rural and more urban. Although urban areas occupy less than 3% of the planetary landmass, they are the foci of humans and economic activity. The climates that they generate are distinctive and represent unambiguous evidence of the anthropogenic climatic effect. This urban climate effect is a consequence of two related properties, land cover (form) and land use (function). Urbanisation replaces 'natural' surfaces with manufactured materials that are usually impervious and have distinctive thermal and radiative properties. In addition, the urban surface is both geometrically complex and highly diverse. These properties of form result in the formation of myriad microclimates caused by a number of climate drivers, including access to the sun and shelter from wind. Urban function refers to the human activities that generate waste heat, moisture and materials as a result of transportation, industrial production, energy consumption, and so on. These functions tend to have distinctive spatial and temporal emission patterns. Together, urban form and urban function generate urban climates at a hierarchy of scales.

At a micro-scale, the outdoor climate is extraordinarily diverse and a myriad of microclimates are generated in and around buildings. Turbulence mixes these distinct climates so that, with increasing elevation, the individual contributions become diluted and the urban (rather than building) climatic effect becomes evident. This mixing process produces an urban boundary layer (UBL) that develops at the upwind edge of the city and grows in depth with distance as it entrains non-urban air into the layer at its upper boundary (Figure 1). For a large city, the UBL may be 1-2 km deep by late afternoon as surface heating by the sun encourages vertical exchanges. At the lee side of the city a new boundary layer forms and it too grows in depth with distance from the city edge. It will develop as an internal boundary layer separating the elevated UBL from the underlying surface. As a result an urban plume,

* Gerald Mills, School of Geography, Planning, and Environmental Science, University College Dublin.

which is warm, relatively dry and enriched with a host of gaseous (including CO₂) and material pollutants, extends downwind of the city. An understanding of the growth and development of the UBL is necessary for a range of climatic studies, including the formation of the urban heat island and local and regional air quality. This paper reports on a project that is examining Dublin's climate by measuring energy exchanges at the urban surface. However, identifying this 'surface' is not easy in an urban setting. A brief discussion into boundary-layer climatology will make the urban 'problem' clearer and provide a context for the research reported on here.

Figure 1. Schematic of the vertical layers at which urban climate effects occur. The urban boundary layer is generated as a result of the urban form and function and can extend downwind of the city. The arrow indicates the direction of the prevailing wind



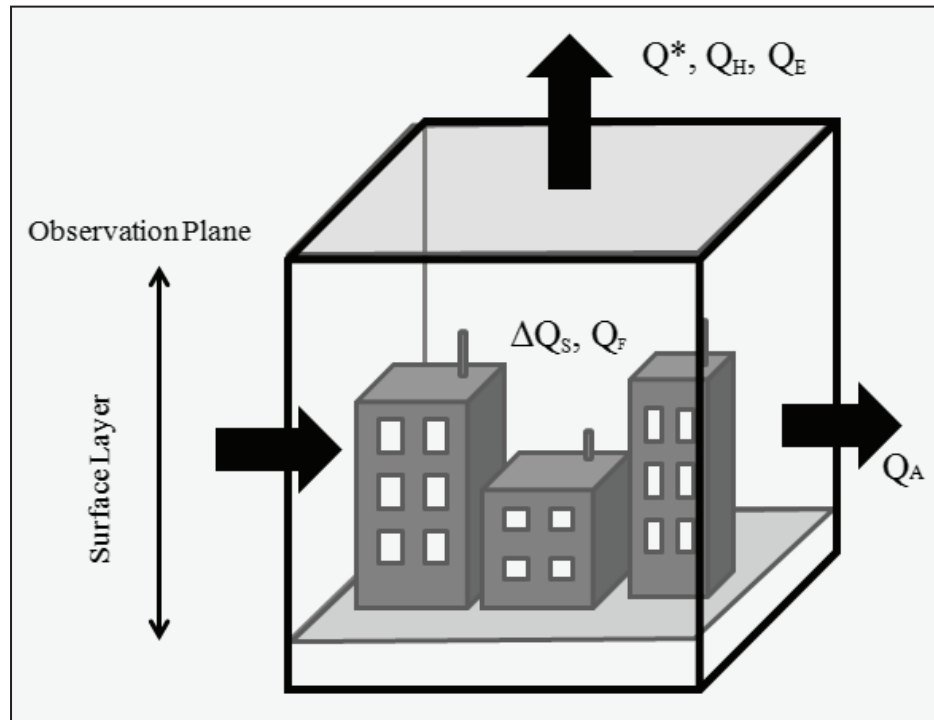
Boundary-layer climatology

The climate near the ground is formed as a result of energy exchanges with the underlying surface, which can be formalised as a statement on the energy budget that may be applied to a volume (Fig 2),

$$Q^* = Q_H + Q_E + \Delta Q_S + \Delta Q_A \quad (1)$$

Net radiation (Q^*) is partitioned into the vertical exchange of sensible and latent heat (Q_H+Q_E) via turbulence, the storage of heat (ΔQ_S) and the horizontal transport of energy or advection (ΔQ_A). Each term is expressed as a flux density, the flow of energy per unit surface area (Wm^2). If these terms are measured over a homogenous surface then there is no horizontal transfer in the system and $\Delta Q_A \approx 0$. In these circumstances, the only concern is the height at which the remaining terms are evaluated. Ideally, the observation platform is located within a constant flux layer where each of the energy budget terms is nearly invariant with height. This layer represents the level at which the atmospheric properties have come into equilibrium with the surface below. It is located above the height of the roughness elements, which may be blades of grass on a prairie or trees in a forest.

Figure 2. Schematic of a typical urban volume illustrating the required height at which to make representative observations. The vertical arrow represents vertical exchanges of energy via turbulence, and the horizontal arrows represent the transfer of energy via advection



Net radiation (Q^*) is comprised of the incoming (\downarrow) and outgoing (\uparrow) short- (K) and longwave (L) radiation,

$$Q^* = K \downarrow - K \uparrow + L \downarrow - L \uparrow \quad (2)$$

Shortwave (or solar) radiation is emitted by the sun, it occupies a wavelength range between 0.01 and 3 μm and has a peak at about 0.5 μm within the spectrum of visible radiation. Incident shortwave radiation ($K\downarrow$) at a surface is a function of day of year and time of day, which govern the altitude of the sun in the sky. In Ireland maximum $K\downarrow$ (approx. 800 Wm^{-2}) will occur on a flat surface at noon under a clear sky during the summer solstice. At noon on a clear winter day, the magnitude of $K\downarrow$ will be a great deal less (approx. 300 Wm^{-2}). Time of year also controls the length of day, whereas during the summer solstice the day-length in Dublin is 17 hours, at the time of the winter solstice, it is just 7.5 hours. Outgoing shortwave radiation ($K\uparrow$) is a function of a surface reflectivity (or albedo) which is expressed as a proportion (α),

$$K \uparrow = K \downarrow \alpha \quad (3)$$

Albedo varies with surface cover and common values are listed in Table 1.

Table 1. Thermal properties of grass and materials used in urban construction (Modified from Oke, 1987).

Material	Emissivity	Albedo	Density (kg m ⁻³ x 10 ³)	Conduc- tivity (Wm ⁻¹ K ⁻¹)	Heat capacity (Jm ⁻³ K ⁻¹ x 10 ⁶)
Concrete	0.71-0.90	0.10- 0.35	2.40	1.51	2.11
Asphalt	0.95	0.05- 0.20	2.11	0.75	1.94
Tile	0.90	0.10- 0.35	1.92	0.84	1.77
Slate	0.90	0.10	2.69	2.01	2.06
Glass	0.87-0.94	0.08	2.48	0.74	1.66
Brick	0.90-0.92	0.20- 0.40	1.83	0.83	1.37
Stone	0.85-0.95	0.20- 0.35	2.68	2.19	2.25
Grass	0.95	0.26	-	-	-

Longwave (or terrestrial radiation) is that emitted by all objects at Earth-like temperatures. It occupies a range between 3 and 30 μm and has a peak at approximately 10 μm . The magnitude of emitted radiation is a function of both temperature and emissivity (ϵ). For a surface, incoming longwave radiation ($L\downarrow$) is derived from the overlying atmosphere,

$$L\downarrow = \epsilon_a \sigma T_a^4 \quad (4)$$

Where T_a is air temperature (in Kelvin, K), σ is the Stefan-Boltzmann constant ($5.67 \times 10^{-8} \text{ Wm}^{-2}\text{K}^{-4}$) and ϵ_a is atmospheric emissivity, which is substantially a function of atmospheric water content. Outgoing longwave radiation ($L\uparrow$) is comprised of that which is emitted and reflected $L\downarrow$,

$$L\uparrow = \epsilon_s \sigma T_s^4 + (1 - \epsilon_s)L\downarrow \quad (5)$$

where the subscript (s) refers to the surface. Emissivity varies with the nature of surface materials – most natural surfaces have ϵ_s values greater than 0.9 (see Table 1).

Over the course of a day, each of these radiation terms inscribes a distinctive pattern. In the absence of cloud, $K\downarrow$ increases from sunrise to noon and declines until sunset and $K\uparrow$ displays an opposite pattern. At night both are zero. By comparison the longwave terms show little diurnal variation and typically $L\uparrow$ exceeds $L\downarrow$. Net radiation (Q^*) then is

negative at night and positive during the daytime. This energy is used to drive heat transfers with the overlying atmosphere and underlying soil.

Vertical heat exchanges with the atmosphere occur as turbulent motions transfer sensible and latent heat. These occur as a consequence of vertical gradients of air temperature and humidity. The nature of these exchanges can be represented simply as,

$$Q_H = -C_a(\overline{w'T'}) \text{ and } Q_E = -L_v(\overline{w'\rho'_v}) \quad (6 \text{ and } 7)$$

Where C_a is the heat capacity of air and L_v is the latent heat of vapourisation (L_v), which may be treated as constant near the surface. The terms in the parenthesis represent the correlation of vertical velocity (w) and air temperature (T) and of w and humidity (q_v). The overbar represents an average and the primes represent fluctuations (positive and negative) from that average. It is the correspondence of the signs of deviation that produces a positive or negative flux. For example, if a rising ($w' > 0$) brings warmer air ($T' > 0$) then the flux is positive, similarly if sinking air ($w' < 0$) brings warmer air ($T' > 0$), the flux is negative.

The final term in the equation is heat storage, which refers to the energy stored in the volume under study. A small proportion of this heat is stored in the atmosphere and is revealed as changes in the vertical air temperature and humidity profiles that result from surface-air exchanges. The majority however is stored in the solid substrate, the layer below the surface. The lower boundary of the volume under study extends to a depth (D) where no diurnal temperature change occurs so that,

$$\Delta Q_s = DC_s \frac{\Delta T}{\Delta t} \quad (8)$$

Where C_s is the heat capacity ($\text{Jm}^{-3}\text{K}^{-1}$) of the substrate and $\Delta T/\Delta t$ is the change in temperature with time (Ks^{-1}).

When these terms (Q^* , Q_H , Q_E and ΔQ_s) are plotted over the course of a day each flux exhibits characteristic patterns that illustrate the nature of exchanges. The net radiation curve is negative overnight and positive during the day, which corresponds to daytime radiative heating (associated with the receipt of short-wave radiation) and night-time radiative cooling. At night this cooling is supported by heat drawn out of storage and by heat transfer from the overlying atmosphere. During the daytime, the opposite occurs as the surplus energy at the surface is used to heat the atmosphere and the substrate. However, the patterns are not symmetrical about noon. When the sun rises and Q^* becomes positive, most of this energy initially is transferred into the substrate. At this time of the day the atmosphere near the surface is very stable and there is little turbulent activity. As the surface continues to warm the near-surface air temperature gradient increases, vertical motion becomes more vigorous

and Q_H and Q_E begin to dominate exchanges. By the afternoon, ΔQ_s has become negative (heat drawn out of storage), even though Q^* is still positive. Q_H and Q_E remain positive even after sunset, when Q^* has become negative.

This outline describes a typical pattern on a sunny calm day, where vegetation is present. On a cloudy day, there is little direct beam short-wave radiation to drive the diurnal patterns and the atmospheric response is muted. Similarly, on a windy day turbulence is driven by mechanical forces and the nature of energy partitioning between the atmosphere and the substrate changes. In these circumstances, one would expect the atmospheric temperature profile to be neutral (isothermal) as heat is mixed into a deep layer. Finally, the nature of exchanges will depend upon the nature of the surface itself. For example, in the absence of vegetation, there will be little potential for evaporation and Q_E will be small. In these circumstances available radiation energy (Q^*) is partitioned into heating the atmosphere (Q_H) and the substrate (ΔQ_s). A common means of comparing surface types then is to obtain the ratio of energy fluxes to see how available net radiation energy is partitioned in storage ($\Delta Q_s/Q^*$) or among the turbulent fluxes (Q_H/Q_E).

The urban problem

Cities pose a real challenge for the application of boundary-layer concepts largely owing to the nature of urban functions and of urban form. As a result there are very few measurements programmes internationally of any duration. Nevertheless, the results from these programmes have provided the conceptual basis for observations within the urban environment and are used in the project described here.

The effect of urban functions is the emission of an anthropogenic heat flux (Q_F) that can be substantially attributed to energy use associated with industrial production, building air conditioning (e.g. heating, cooling and lighting) and transportation. It represents an additional term in the energy budget (EB) equation,

$$Q^* + Q_F = Q_H + Q_E + \Delta Q_s + \Delta Q_A \quad (9)$$

Q_F is difficult to isolate in measurement programmes and is most often estimated from information on energy use. For mid-latitude cities it is estimated at between 25-100 Wm^{-2} on average depending on the intensity of energy use in different parts of the city. It will also have a distinctive temporal pattern associated with the working day and week. As an aside, as most energy is generated from fossil fuels, Q_F is directly linked to the emission of CO_2 in cities.

The effect of urban form is twofold. Firstly, the urban surface is aerodynamically very rough and this is reflected in a deep layer of intense turbulent activity that creates a deep surface layer. Secondly, the urban

facets that comprise the urban surface (walls, roofs, gardens, etc) are highly diverse in terms of their radiative and thermal attributes. The result is exceptional micro-scale variation in atmospheric properties (wind, temperature, humidity, etc.) in and around buildings so that observations close to buildings will have difficulty in ‘closing’ the energy budget owing to the diverse sources from which the instruments will sample. In these circumstances, observations that are representative of the underlying urban surface (with its characteristic diversity) need to be made at a height where these microscale variations have become blended. The evidence from field observations suggests that energy flux instruments should be placed at 1½ to 2 times the average height of buildings to avoid the effects of individual buildings and surfaces.

Finally, we must deal with the issue of surface variation, which means advection cannot be ignored ($\Delta Q_A \neq 0$). Although the urban surface is heterogeneous, much of this variation can be attributed to variation between types of urban landscapes that are (relatively speaking) extensive and homogenous. Thus, for example, mature residential suburbs in Ireland can be characterised by typical residential densities, building dimensions, road widths, green areas and so on. Similarly, industrial, commercial or city centre have characteristic properties associated with form and function. From this perspective the urbanised surface can be seen as a patchwork of urban sub-types. As air moves across the city surface, it encounters different patches and each of which will modify the overlying air. Initially, at the boundary between one sub-type and another, these modifications are significant as the air rapidly adjusts to changes in the underlying surface. These effects are transferred upwards into the atmosphere forming an internal boundary layer that grows in height at a rate of about 1:100. In other words, air traversing a distinctive urban surface will have an internal boundary layer approximately 10 m thick, 1 km from the upwind edge of that patch (termed the ‘fetch’). At an urban scale, each of these internal boundary layers become progressively mixed with vertical distance from the urban surface until the unique imprints of the urban subtypes is lost.

To apply the EB to these urban sub-types requires that the instrument platform is both within the fetch of that sub-type and near the top of the surface layer. In these circumstances, the observations will sample from air that has been uniquely affected by the underlying surface at a height where the variations associated with that urban-subtype have been thoroughly mixed. Ideally this is accomplished by identifying urban patches that are representative of an urban sub-type and extensive in area, and locating an observation platform at 1½ to 2 times the average height of buildings and sufficiently distant from the boundary of that patch.

This research that is reported on here is the first examination of the energy budget of Dublin's urban surface. It will contribute to a growing number of urban energy budget programmes globally.

Methodology

Two locations were identified in Dublin to represent two urban subtypes: suburban and urban (Figure 4). The suburban site is located in residential Terenure in south-west Dublin and consists of semi-detached, two storey houses with large private gardens. The observation site is on the grounds of a primary school and the instrument platform is placed on a mast at a height of 12 m whereas the average building height is 8 m. Land use here is predominantly residential and light commercial activity and natural land cover consists of gardens, shrubbery and mature trees. The urban site is located on the western side of inner city Dublin where the instrument platform is attached to a mast on a three-storey building, 17 m above ground-level. The surrounding building heights range from 4.5 m to 18 m, but the mean height is about 10 m. The principal land uses are industrial, light-commercial, residential and institutional. Located to the south, east and west of the instruments are a combination of storing yards, warehouses, car parks, and institutional buildings. To the north of the observation site are two- to five-storey residences consisting of both apartments and houses and the Guinness brewery.

A combination of site surveys, aerial imagery and a geographic information system (GIS) was used to determine the physical properties of the observation sites (Table 2). Information regarding instrument height, orientation and exposure was determined and recorded at the time of deploying the instruments. Dublin City Council (DCC) provided a vector-based GIS dataset representing estimated building heights in metres for the urban site and a site survey was conducted at the suburban site. Digitised datasets illustrating different surface covers such as, asphalt, concrete and vegetation, were created for both observation sites and were used to derive area-average albedo and emissivity values using information from a circular area (radius 200 m) centred on each site. For the suburban site, values for albedo ranged from 0.17 to 0.28 and those for emissivity ranged between 0.87- 0.92. By comparison, the urban site which had less green area, exhibited values for albedo and emissivity values of 0.10-0.25 and 0.76-0.80 respectively.

At each site a suite of high-resolution micro-meteorological instruments is deployed (Table 3 and Fig 6a). Net radiation (Q^*) and its short- and long-wave components are obtained from an instrument that records radiation receipt on an up- and down-facing pyranometer (K_{\downarrow} and K_{\uparrow}) and pyrgeometer (L_{\downarrow} and L_{\uparrow}). The turbulent fluxes of sensible (Q_H) and latent (Q_E) heat fluxes are obtained using an open-path eddy covariance (EC) system, which comprises a sonic anemometer (which measures vertical velocity, w) combined with fast response temperature (T) and humidity (q_v) sensors (Table 3 and Plate 2). Measurements are made at a

rate of once each 0.1 s and from this 30 minute averages and deviations (w' , T' and Q_v') are obtained, see eqn. 6 & 7. This data forms the basis of the calculation of the turbulent energy fluxes. The anthropogenic heat flux (Q_F) is not explicitly measured here and is included within ($Q_H + Q_E$) and we do not attempt to obtain this term separately. The remaining flux in the energy balance is ΔQ_S , which is heat held in storage. Again, this is not obtained directly here and is estimated as the residual from eqn. 10,

$$\Delta Q_S \approx Q^* - (Q_H + Q_E) \quad (10)$$

One should note that in this formulation ΔQ_S includes any measurement errors associated with the terms on the RHS. These errors result from both instrument and observational inaccuracies. The latter are particularly difficult to quantify as they result from the different source areas that the instruments sample from. For example, while the radiation instruments obtain their fluxes from a circular area directly below the mast, the turbulent fluxes vary in space and time associated with wind velocity and atmospheric stability. These errors are greatest when the underlying surface is heterogeneous.

In this paper we evaluate the magnitude of errors in ΔQ_S by comparing values obtained as a residual from eqn. 11 against those derived using the objective hysteresis model (OHM) developed by Grimmond et al (1991). While this does not address the errors associated with varying source areas, it does provide some confidence in our calculated storage terms and indirectly in the turbulent flux terms. In a subsequent paper the source areas of the Q_H and Q_E will be presented. The OHM estimates ΔQ_S as a function of net radiation and the thermal properties of the surrounding urban surface,

$$\Delta Q_S = \sum_{i=1}^n \left[a_{1i} Q^* + a_{2i} \frac{\Delta Q^*}{\Delta t} + a_{3i} \right] \quad (11)$$

Where n refers to each of the i surface types that are found in a 200 m radius area surrounding the observation platform where Q^* is measured and the terms a_1 , a_2 and a_3 are coefficients obtained from previous studies (Table 4). The average values of these coefficients are used here in conjunction with surface cover statistics to calculate site specific model coefficients (Table 4 and 5). OHM values are then compared with residual values to evaluate the EB.

Figure 3. Planar area illustrating the surface covers of the 200 metre radius surrounding (a) suburban and (b) urban observation sites. Building footprints were provided by Ordnance Survey Ireland, Government of Ireland (EN 0063512).

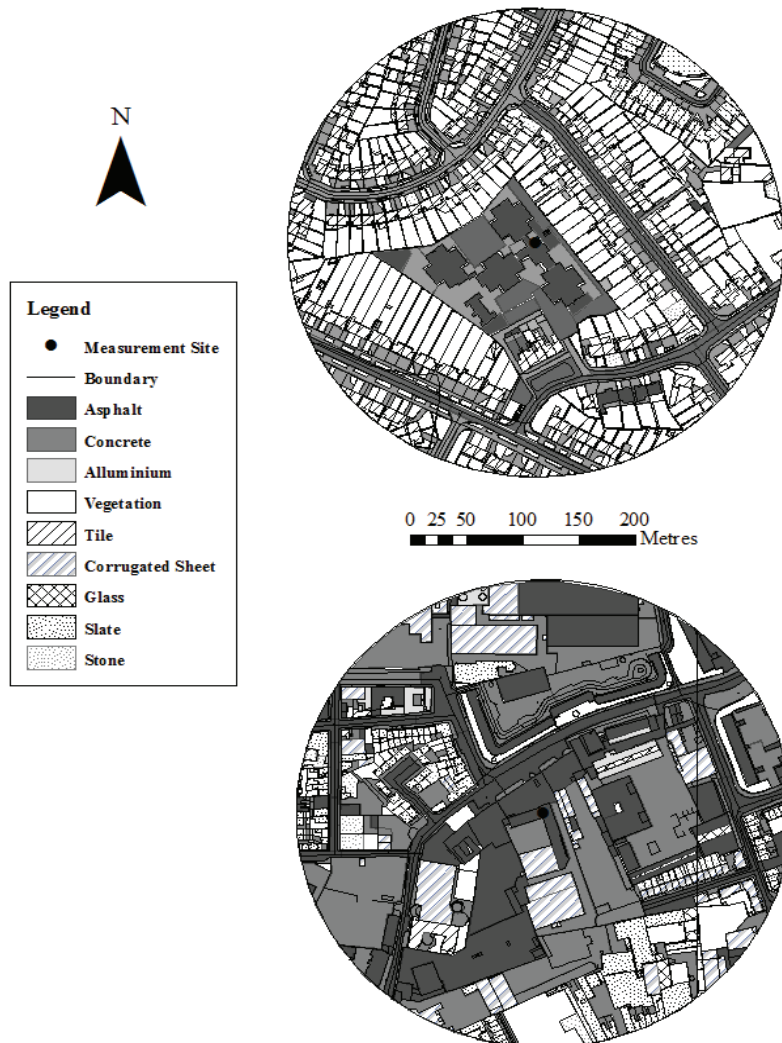


Table 2. A) Shows the fractional surface cover and B) outlines the physical properties of the observation sites.

(A) Surface cover				
Site	Roof	Asphalt	Concrete	Vegetation
Urban	0.24	0.22	0.44	0.10
Suburban	0.22	0.10	0.25	0.43
(B) Physical properties				
Site	Albedo	Emissivity	Building height	Building aspect ratio
Urban	0.10-0.25	0.76-0.8	10 metres	0.40
Suburban	0.17-0.28	0.87-0.92	8 metres	0.30

Figure 4. Google earth images representing a 1km radius of the observation sites, the black arrows represent the south westerly wind direction prevailing during the observation campaign.

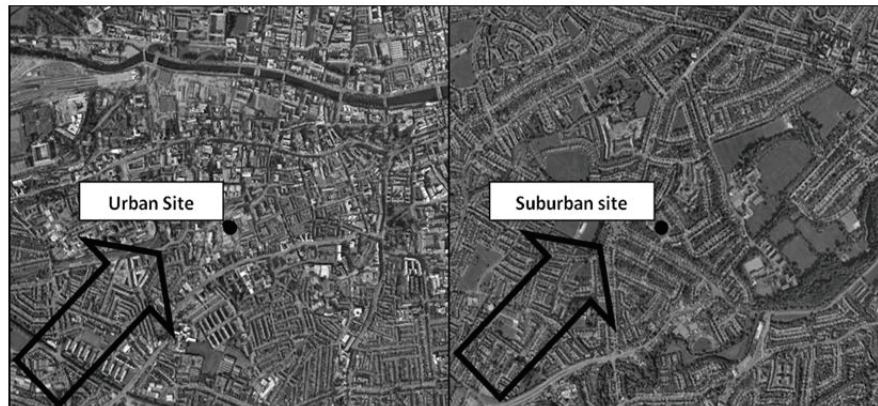


Figure 5. Mean daily mean sea level pressure in Pascals for a) 17 April 2010 and b) 20 June 2010. Source: National centres for environmental prediction (NCEP) reanalysis data.

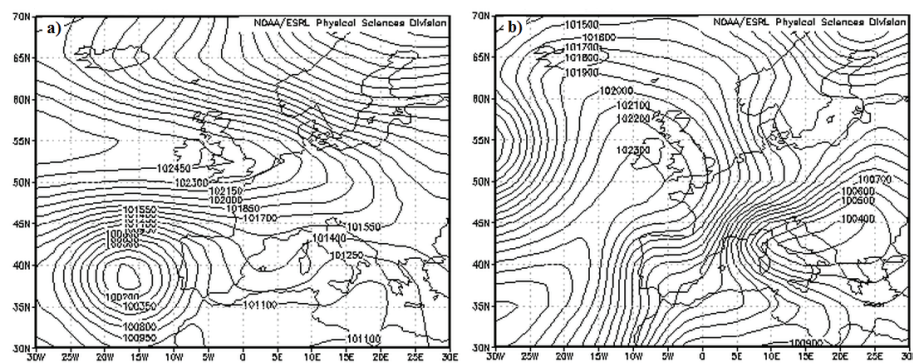


Figure 6. a) Instruments mounted at the suburban site, b and c illustrate the difference in vegetation density between April and June 2010 at the suburban site.

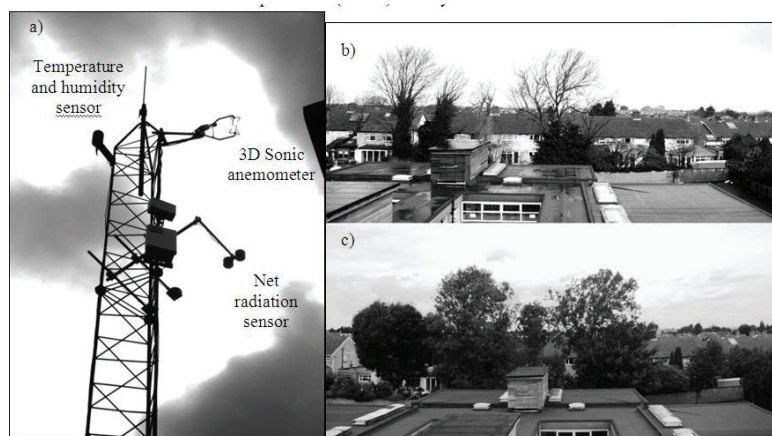


Table 3. Variables measured, instrument name and manufacturer and instrument height (z) above ground-level

<i>Variable</i>	<i>Urban</i>	<i>Suburban</i>
Net all-wave radiation	Net radiation sensor, Hukseflux, NR01 z=15m	Net radiation sensor, Hukseflux, NR01 z=11m
Wind velocity in x, y and z directions	Sonic anemometer, Campbell Scientific, CSAT3, z=17m	Sonic anemometer, Campbell Scientific, CSAT3, z=12m
Water vapour density	IRGA, Licor Sciences, LI-7500, z=17m	IRGA, Licor Sciences, LI-7500, z=12m
Air temperature and relative humidity	Temperature and relative humidity probe, Vaisala Inc., HMP45C, z=17m	Temperature and relative humidity probe, Vaisala Inc., HMP45C, z=12m

Table 4. Empirically derived coefficients used in the OHM and their authors

<i>Surface cover</i>	<i>Author</i>	<i>Regression coefficients</i>		
		a_1	$a_2 (b)$	$a_3 (Wm^{-2})$
1. Vegetation				
Grass	(Doll et al. 1985)	0.32	0.54	-27.4
2. Rooftop				
Uppsala	(Taesler 1980)	0.44	0.57	-28.9
Vancouver	(Yap 1973)	0.17	0.10	-17
Kyoto	(Yoshida et al. 1990-91)	0.82	0.34	-55.7
	Average	0.4766	0.3366	-33.8666
3. Paved/Impervious				
Concrete	(Doll et al. 1985)	0.81	0.48	-79.9
	(Asaeda et al. 1996)	0.85	0.32	-28.5
	Average	0.83	0.40	-54.2
Asphalt	(Narita et al. 1984)	0.36	0.23	-19.3
	(Asaeda et al. 1996)	0.64	0.32	-43.6
	(Anandakumar 1999)	0.82	0.68	-20.1
	Average	0.6066	0.4100	-27.6666

Table 5 A) and B) Employ the averages of the regression coefficients and the surface cover weighting factors to calculate site specific model coefficients

A) OHM coefficient calculation for the suburban site				
Surface cover	Weighting factor	a ₁	a ₂	a ₃
Greenspace	0.43	0.1376	0.2322	-11.7820
Rooftop	0.22	0.1034	0.0208	-7.4580
Concrete	0.25	0.2075	0.1	-13.5500
Asphalt	0.10	0.061	0.0410	-2.7670
Model coefficient		0.5095	0.3940	-35.5570

B) OHM coefficient calculation for the urban site				
Surface cover	Weighting factor	a ₁	a ₂	a ₃
Greenspace	0.10	0.032	0.054	-2.7400
Rooftop	0.24	0.1128	0.0816	-8.1360
Concrete	0.44	0.3652	0.1760	-23.8480
Asphalt	0.22	0.1342	0.0902	-6.0874
Model coefficient		0.6442	0.4018	-40.8114

Table 6. Average of radiation fluxes for April 17th and June 20th for the observation sites. Average values for K_↓ and K_↑ pertain to daylight hours while average values for L_↓ and L_↑ pertain to all 24 hours

Month	Site	K _↓	K _↑	Albedo (a)	L _↓	L _↑
April	Urban	363.43	48.58	0.14	291.30	389.54
April	Suburba n	372.07	34.18	0.10	294.29	392.73
June	Urban	511.80	64.03	0.13	318.20	426.25
June	Suburba n	510.61	45.01	0.10	319.48	435.06

Table 7. Proportioning of net radiation (Q*) for daytime- and all-hours for the two observation sites

Month	Site	Hours	Q*	Q _H /Q*	Q _E /Q*	ΔQ _S /Q*	Q _H /Q _E	Q _H /ΔQ _S
				χ	γ	Λ	β	κ
April	Sub-urban	All hours	139.62	0.51	0.12	0.37	4.09	1.38
		Q* > 0	333.56	0.44	0.10	0.46	4.40	0.97
	Urban	All hours	122.81	0.59	0.03	0.37	17.82	1.60
June	Sub-urban	Q* > 0	327.70	0.43	0.02	0.55	21.32	0.78
		All hours	212.94	0.48	0.15	0.37	3.14	1.29
	Urban	Q* > 0	388.62	0.44	0.13	0.43	3.31	1.02
		All hours	207.51	0.59	0.07	0.34	8.66	1.73
		Q* > 0	410.30	0.46	0.04	0.49	10.52	0.94

Figure 7. The diurnal profile of the radiation balance of the suburban observation site for April 17th 2010.

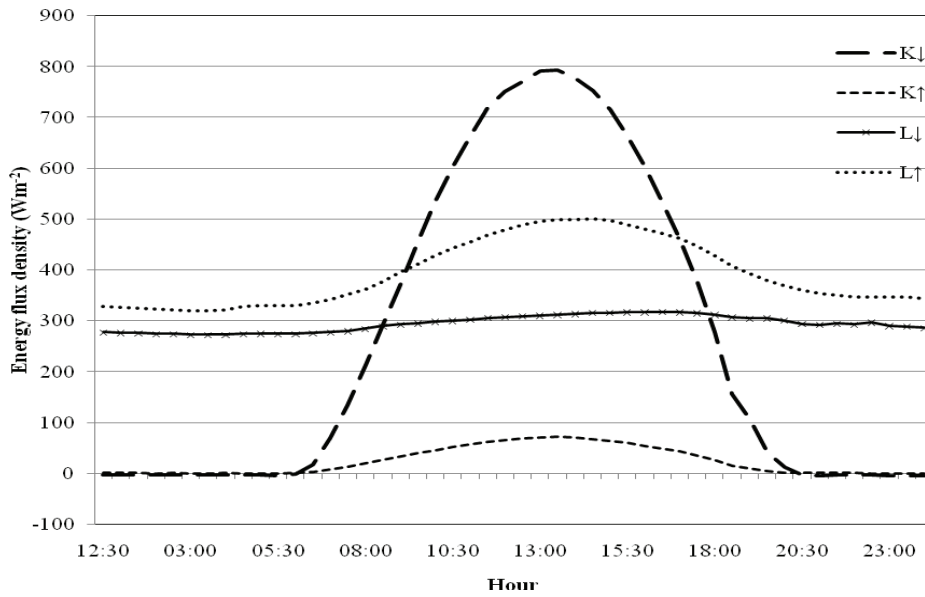
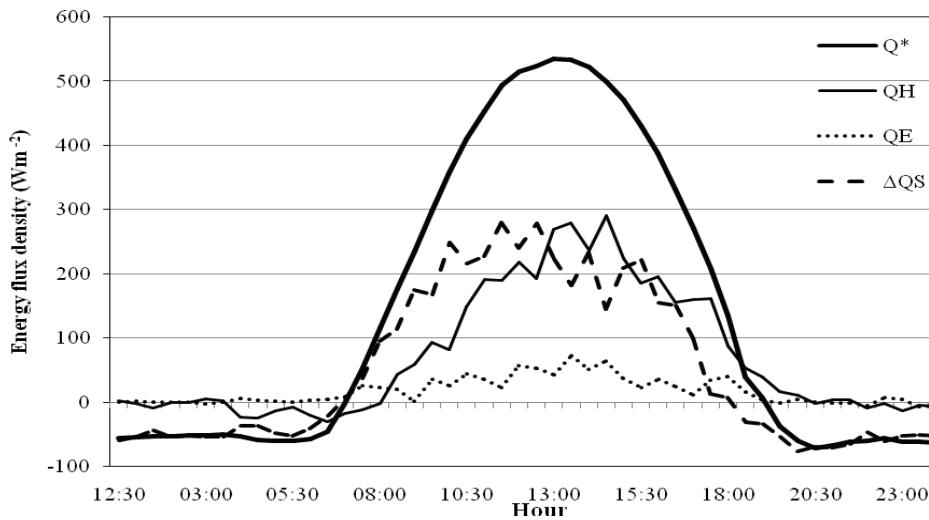


Figure 8. The diurnal profile of the surface energy balance of the suburban observation site for April 17th 2010.



Results

As the purpose of this investigation is to examine the distinctive urban climatic effect, two days were selected for an initial investigation that reported clear-sky and calm conditions, which were likely to accentuate this distinction. The meteorological conditions on April 17th and on June 20th 2010 were consistent; clear-skies, wind speeds below 5ms^{-1} from a south-westerly direction ($200\text{-}240^\circ$). Meteorological conditions were also

associated with high pressure systems centred on, or close to, Ireland and both days followed dry periods.

The radiation budget

The radiation budget (RB) for April 17th at suburban location is presented in figure 7 and illustrates the diurnal profile of incoming and outgoing/reflected solar and longwave radiation. The results are half-hourly averages and are corrected to local apparent time (LAT). K_{\downarrow} has a distinctive pattern during clear-sky conditions in that it is symmetrical around solar noon. For April 17th K_{\downarrow} increases following sunrise (06.30), peaks at solar noon (794 Wm^{-2} at 13.30) and declines in magnitude, in unison with solar elevation, before becoming zero at sunset (20.30) (Fig 7).

K_{\uparrow} is a function of K_{\downarrow} and the surface albedo. As K_{\downarrow} increases with solar elevation a greater proportion is reflected by the surface, this gives rise to a peak in K_{\uparrow} at solar noon (72 Wm^{-2}) (Fig 7). In the absence of solar inputs both K_{\downarrow} and K_{\uparrow} are zero during the night time. During cloudy conditions K_{\downarrow} and consequently K_{\uparrow} would not exhibit a smooth curve like that in figure 7. Instead the flux would vary according to cloud passing over the radiation sensor. In this case a greater portion of solar radiation would be received via diffuse as oppose to direct beam solar radiation. As mentioned earlier fluxes of L_{\downarrow} are a function of the temperature and emissivity of the overlying atmosphere. Fluxes are the lowest in magnitude from midnight until sunrise. During this time the overlying atmosphere of the suburban location continues to cool in the absence of solar inputs, consequently temperature and L_{\downarrow} decrease. Throughout the daytime the atmosphere begins to heat up and values are greatest during the late afternoon (317 Wm^{-2} at 16.30). L_{\uparrow} on the other hand is a function of the temperature and emissivity of the surface beneath the radiation sensor and that which is emitted and reflected L_{\downarrow} . The suburban surface responds more efficiently to changes in temperature than the overlying atmosphere, especially for a location whose surface extent is largely made up of greenspace or grass. In this case the surface will heat up and cool down in close conjunction with the magnitude of K_{\downarrow} (Fig 7).

In order to investigate the RB over space a brief overview of results will be outlined for the urban location for this day. Firstly values representing K_{\downarrow} were similar in magnitude to the suburban location throughout the daytime. K_{\downarrow} is largely governed by external factors (i.e. latitude and solar inclination) therefore one would expect the two locations, located within 5km of each other, to receive similar amounts of solar radiation. Peak K_{\downarrow} was 777 Wm^{-2} whilst peak K_{\uparrow} was 104 Wm^{-2} . Lower values for K_{\downarrow} for urban locations relative to suburban locations are reported in the international literature and are attributed to increased pollution concentration which serves to reduce irradiance (Jauregui and Luyando, 1990, Stanhill and Kalma, 1995). With regard to K_{\uparrow} dense urban

locations generally possess lower albedos than those of suburban locations. This investigation revealed higher values of $K\uparrow$ for the urban location indicating a higher surface albedo. This trend was unusual given the nature of the two measurement locations and will be discussed later. Similarly longwave radiation fluxes showed deviations from its suburban counterpart. Urban materials generally have lower emissivities than grass and take longer to heat up. As a consequence $L\uparrow$ increases later in the day than its suburban counterpart. Thus daytime values are lower in magnitude whilst night time values are consistently greater in magnitude than the suburban location. Values pertaining to the urban location for $L\downarrow$ are almost identical to those observed at the suburban location and again reflect the relatively spatial consistency of in-coming radiation fluxes. The RB for June 20th revealed much the same patterns for $K\downarrow$, $K\uparrow$, $L\downarrow$, and $L\uparrow$ at the two measurement locations. The magnitude of solar radiation increased relative to April 17th as a result of increased solar inclination towards the sun, which in turn increased the day length and hours where solar radiation was received by the surface. Peak values for $K\downarrow$ increased by more than 100 Wm^{-2} at the two locations, with corresponding increases in the magnitude of $K\uparrow$, $L\downarrow$, and $L\uparrow$. Average radiation values across the two locations for the measurement days are outlined in table 6.

The surface energy balance

The EB corresponding to the suburban location during April 17th is illustrated in figure 8. The EB represents the expenditure of net radiant energy (Q^*) between surface heat fluxes (Q_E , Q_H , and ΔQ_S). The timing, partitioning and magnitude of these surface heat fluxes are determined by the nature of the underlying surface, for example the availability of water for evaporation or the presence of substrate for storage. The smooth pattern of Q^* illustrates the increase of net radiant energy into the local climate system in response to solar inputs ($K\downarrow$ in figure 6). Peak Q^* occurs around solar noon and declines thereafter becoming negative in magnitude around sunset (approx 20:30 in April) (Fig 8). Storage heat is the first of the heat fluxes to increase following sunrise a trend that has also been observed in previous international studies (Grimmond and Oke, 1999, Christen and Vogt, 2004). Following sunrise energy is directly transferred into the substrate at the observation site and ΔQ_S is the dominant heat flux in the morning. ΔQ_S is the first heat flux to become negative, changing sign prior to sunset; this trend illustrates the release of heat from the substrate to the atmosphere via Q_H . Also evident in the diurnal trend of ΔQ_S is a double peak, occurring around 13:00 and 15:30. As solar elevation declines energy is transferred to previously shaded facets giving rise to this second peak in ΔQ_S . Following noon Q_H becomes the dominant heat flux for the afternoon and evening where heat energy is preferentially channelled into the atmosphere via turbulence as oppose to the substrate via conduction (Fig 8). Surface warming occurring in the morning causes vertical temperature gradients to develop and encourages turbulent mixing in the surface layer. In the

absence of solar input via K_{\downarrow} sensible heat decreases at night and the atmosphere continues to cool until the morning (Fig 8). Q_E representing fluxes of latent heat are lower in magnitude relative to values pertaining to ΔQ_S and Q_H . Fluxes of Q_E are influenced by water availability, and the presence and density of natural surface cover which in turn determines the available surface for transpiring and evaporating. Low vegetation density in conjunction with dry antecedent conditions in April would have affected the availability of surface area and water for evaporation and hence fluxes of Q_E . That said however the diurnal trend largely follows that of Q_H and Q^* , increasing following sunrise, peaking in the afternoon (73 Wm^{-2}) and decreasing thereafter (Fig 8).

Difference of the EB over space: April 17th

Within the two study volumes the magnitude and timing of available radiant energy (Q^*) is very similar. Peak values occur at 13.00 and are 535 and 541 Wm^{-2} for the suburban and urban location respectively. Greater night time losses occur at the urban site (approx. -80 versus -60 Wm^{-2}) in response to a greater heat release from the substrate (Fig 9a). Fluxes of sensible heat (Q_H) are driven by surface warming and the consequent convective mixing of warmed air higher into the atmosphere. Q_H is therefore slow to increase and values reach a peak around local solar noon, 290 and 299 Wm^{-2} at the suburban and urban location respectively. Warming of the atmosphere continues into the evening and fluxes can remain positive into the night time. This trend is especially evident at the urban location and gave rise to what is commonly referred to as the nocturnal urban heat island effect (Fig 9b). Fluxes of latent heat are the lowest in magnitude and most variable during the day time at both locations. Fluxes represent the amount of energy spent in the study volume for evaporating water (or adding water to the atmosphere). As mentioned above fluxes at the suburban location increase and decrease in unison with Q^* and the other turbulent flux (Q_H) (Fig 9c). However the urban observations reveal lower values pertaining to Q_E . This trend is expected for a dense urban location that serves to drain water away from the surface and which has a small fraction of greenspace space (10%). The storage heat flux is the most dominant of the fluxes throughout the morning at both locations. Following sunrise heat is quickly and easily transferred to tall building structures. The urban location has a higher storage heat flux during the day time as a result of its higher associated heat capacity (i.e. comprised of more man-made materials) and its greater active surface area (i.e. taller buildings). At night time this trend is reversed and the urban location displays increasingly negative fluxes indicative of greater heat loss from the substrate.

Difference of the EB over time: April 17th versus June 20th

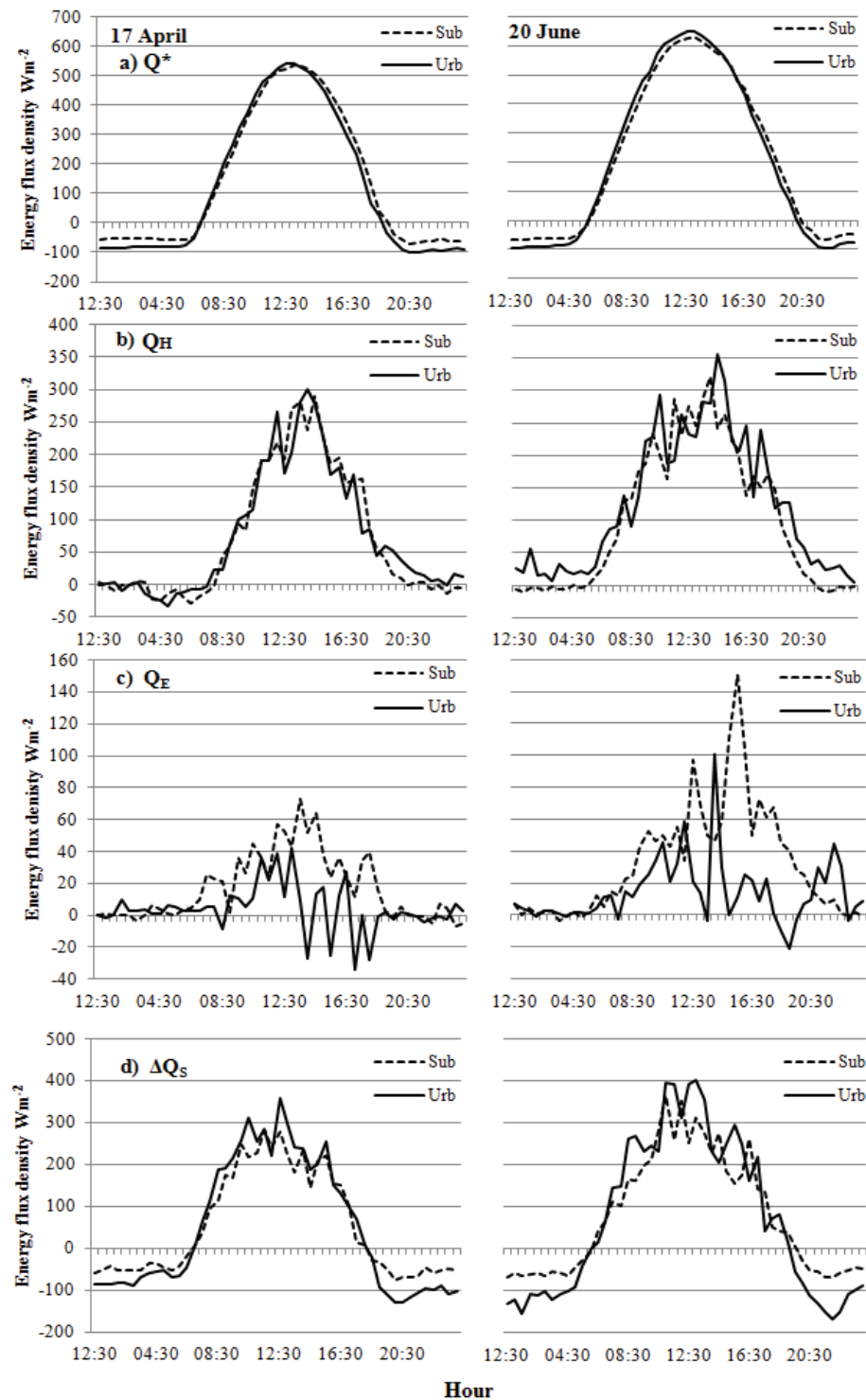
The general trend of Q^* on June 20th does not differ significantly from that observed on April 17th. The increased inclination towards the sun has however increased the day length (affecting the timing) and the maximum possible receipt of radiant energy (affecting the magnitude) at

the surface. Values for Q^* increase earlier in the day and decline later in the evening (Fig 9a), while the peak magnitude increased by 94 and 108Wm^{-2} at the suburban and urban site respectively. Increased day length has also affected fluxes of Q_H . Surface warming occurs earlier in the day hence increasing fluxes of Q_H at the two locations. Peak values increased by 30 and 56Wm^{-2} at the suburban and urban location, and there is more pronounced UHI effect evident at urban location compared to April (Fig 9b). Furthermore the previous day, June 19th, reported clear-sky calm conditions conducive to UHI formation, a trend which can be seen from the fluxes of Q_H at the urban location between midnight and sunrise where values did not fall below zero (Fig 9b). Fluxes of Q_E are again the smallest and most variable of the surface heat fluxes in June. The pattern at the suburban location is more in unison with the other turbulent flux (Q_H) increasing and decreasing with Q^* . The same cannot be said for observations of Q_E at the urban location, where a sharp increase occurs in the late evening (22.00) (Fig 9c) the reason for which is not yet known but may be as a result of an anthropogenic release of moisture into the local system. Peak values of Q_E are significantly greater than those observed in April, increasing by 79 and 59Wm^{-2} for the suburban and urban location respectively (Fig 9c). With regard to average daytime values of at the suburban location Q_E has increased from 33 to 51Wm^{-2} . Although antecedent conditions in June were similarly dry, this increase has been attributed to the vegetation becoming denser thereby increasing the available surface for transpiration and evaporation (Fig 6c). Estimated values pertaining to ΔQ_s increased for June in unison with observed fluxes. Heat is transferred to the substrate earlier in the morning, and although day length has increased ΔQ_s still becomes negative in magnitude prior to sunset at both locations. At the urban location day time values of ΔQ_s are particularly greater while night time values are lower in June relative to April. More heat is channelled into the substrate during the day leading to greater losses at the night (Fig 9d). The heat is lost to the atmosphere via sensible heat, thus helping fluxes of Q_H to remain positive into the night .

Discussion

Given that the heat storage flux, calculated as the residual (ΔQ_{SRES} hereafter), is not an atmospheric or measured variable it will inherently contain errors associated with the measured variables. In order to have confidence in the representativeness and plausibility of the EB results which contain ΔQ_{SRES} , the OHM was employed to generate modelled values for heat storage (ΔQ_{SOHM}) over the measurement campaign. These values are generated using Q^* but are independent of the measured turbulent heat fluxes (Q_E and Q_H) and hence are a useful tool for evaluating the EB residual, ΔQ_{SRES} .

Figure 9. Comparison of urban and suburban surface heat fluxes for 17th April and June 20th 2010. Note the vertical axis scale difference in a, b, c and d.

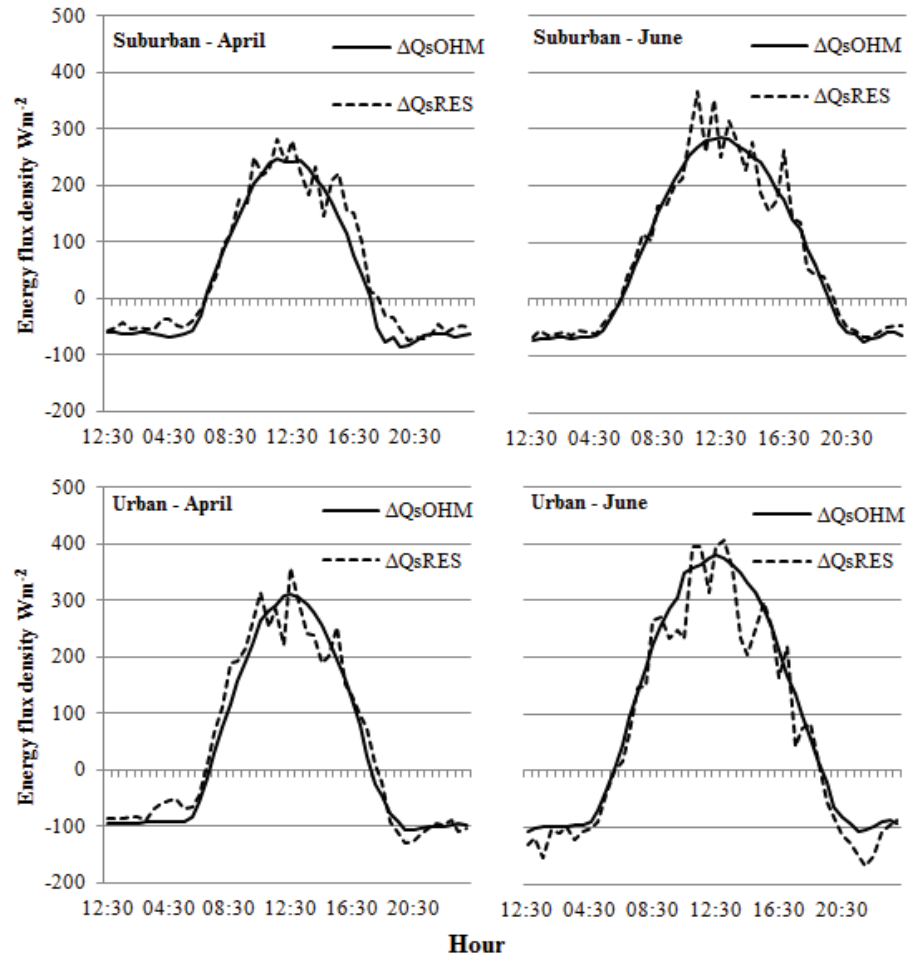


The OHM requires detailed information regarding the fractional cover of surfaces surrounding the measurement location including greenspace, rooftop and impervious (i.e. concrete and asphalt). Each of these surface types have empirically derived coefficients which describe their

1. Direct proportionality to Q^* (a1)
2. Timing in relation to Q^* (which accounts for hysteresis) (a2)
3. Value of ΔQ s when Q^* equals zero (a3).

The coefficients are as a result of previous studies undertaken for urban surfaces and are outlined in table 4. A variety of coefficients are used for each surface type (except greenspace) because their value will be influenced by characteristics of the original study site (Camuffo and Bernardi, 1982). An average of the empirical coefficients is calculated for all but the greenspace or grass surface. In order to calculate site specific model coefficients for the Dublin sites the values of fractional surface cover presented in Table 2 (a) were used in the OHM as land surface weighting factors. The average of each of the surface cover coefficients was then multiplied by the associated weighing factor to generate site specific model coefficients for a1 a2 and a3 (Table 5 a and b). ΔQ_{SOHM} is then calculated according to eqn. 12 for the April 17th and June 20th 2010 and the results are presented in figure10. Overall the EB residuals and modelled values show good agreement regarding the rising and declining limb for all cases (Fig 10). Greater disparity exists however around midday and late afternoon. The OHM is close to estimating peak ΔQ_{SRES} but OHM consistently under predicts values, a trend similar to that reported in Grimmond et al. (1991). Night time values modelled using the OHM are again in good agreement with residuals, particularly at the suburban location. For this investigation residual values were calculated for 30-minute intervals, however Grimmond and Oke (1999) recommend using longer averages (i.e. two hours) especially when dealing with intra-daily data. This would likely improve agreement between values of ΔQ_{SRES} and ΔQ_{SOHM} for a diurnal time series, and in particular around midday. Residual values, although not measured themselves are regarded as the reference values and as the closest to potential correct values given that they are the result of high-grade scientific measurement campaigns (Roberts et al., 2006). Given the good agreement between residual and modelled values it can be assumed that the instruments are observing reasonable EB fluxes for the study campaign. We can therefore have confidence in the EB results as we continue to analyse them in greater detail.

Figure 10. Residual and modelled storage heat fluxes for April 17th and June 20th 2010.



Partitioning of surface energy balance fluxes

Ratios are considered as useful parameters when attempting to identify temporal/diurnal and spatial trends in the partitioning of Q^* . The various ratios are presented in a summary table below (Table 7). The spatial variations in the EB are evident by comparing ratios pertaining to the urban and suburban location. While an increasingly temporal depiction of EB fluxes is provided when ratios are separated into two categories, all hours (i.e. 24hrs) and day time hours (i.e. when $Q^* > 0$). The table outlines the partitioning of available radiant energy (Q^*) into QH, QE and ΔQS and introduces two additional ratios. Firstly, the Bowen ratio (β) describes the relationship between the two turbulent fluxes (QH and QE), when its value is greater than 1 or unity more energy is spent heating the atmosphere than evaporating water. Values of β less than 1 indicate that more energy is used to evaporate or add water to the atmosphere as oppose to adding heat. Secondly, $QH/\Delta QS$ (α) represents the ratio of sensible heat to the atmosphere and to the substrate. When the atmosphere amasses a greater portion of energy than the substrate α

will be greater than 1. Conversely when κ is less than 1 the substrate in the study volume is the more effective energy store.

Latent heat fluxes represent the smallest proportioning of Q^* at the two observation sites in April and June. Q_E accounts for a greater portion of Q^* for all hours than to during day time hours. During the day time other fluxes are more dominant however at night time when storage heat is negative, Q_E can remain positive into the night thus increasing its ratio. Q_E/Q^* increases between April and June for all cases representing the relative increase in fluxes of Q_E in the summer. Maximum Q_E/Q^* occurs at the suburban location in June and represents 15% of Q^* in all hour conditions. Q_H is the greatest consumer of Q^* for all-hours in April and June at both locations, ranging from 44 to 59% of Q^* . This means that over an average 24hr period energy within both systems is predominantly used to heat the atmosphere. Furthermore Q_H/Q^* is consistently greater at the urban location for all hours which means that the urban atmosphere will be relatively drier and warmer than that of its suburban counterpart. The substrate ($\Delta Q_S/Q^*$) is generally the predominant energy sink for day time hours, however ratios are quite similar in magnitude to Q_H/Q^* (Table 7). This trend is reversed for all hours when Q_H/Q^* takes precedence. All hour ratios for $\Delta Q_S/Q^*$ are lower because night time values are negative in magnitude corresponding to losses of heat from the storage substrate.

The Bowen ratio (β) is consistently higher at the urban location for all cases (Table 7). This trend illustrates the significantly lower fluxes of Q_E relative to Q_H . β is greater during day time hours because of the large difference in fluxes of Q_E and Q_H . However β decreases for all hour conditions because of the smaller relative difference in the two turbulent fluxes at night time. β is greater than 1 for all cases indicating that more turbulent energy is used to add heat to the atmosphere as oppose to water. With regard to κ , ratios in Table 7 indicate that the substrate at both locations is the more effective energy sink during the day time (i.e. ratios less than 1). On the other hand for all hour conditions, taking night time values into account, the atmosphere is the dominant store of radiant energy (i.e. ratios greater than 1).

If we return to the RB and recall that the reflected portion of short-wave radiation ($K\uparrow$) at the urban location was unusually greater than that observed at the suburban location; this trend indicated a higher surface albedo at the urban location in comparison to the suburban location. One would expect that the urban environment would have a lower albedo when compared to a well-vegetated suburban location. This unusual trend has been attributed to the nature of the immediate surrounds of the instruments. This area exercises the greatest influence on radiation observations. The Dublin City Council roof and surrounding storage yards are comprised of light coloured asphalt and concrete while the school roof surface and yard are largely made up of darker asphalt.

Darker asphalt would serve to reflect less $K\uparrow$ and hence reduces the surface albedo. The albedo values calculated from the instruments and are presented in table 6. The combined albedos for the observation sites outlined in table 2b are consistent for the urban location (i.e. 0.10-0.25) however the instrument calculated value is outside of the expected range (0.17-0.28) for the suburban location (Table 5a). This indicates that the school yard and roof surface have a greater influence on observations than the extensive greenspace located further from the instruments.

Conclusion

Knowing about the urban landscape, its geometry and surface properties provides researchers with robust explanatory power when deciphering urban meteorological observations. The deployment of high-resolution, meteorological instrumentation in the urban environment has significantly improved our understanding of the energy exchanges operating in the surface layer that give rise to distinctive local climates. The current research was a first attempt at investigating the radiation and surface energy balance for Dublin. This study revealed a spatially conservative radiation budget however the subsequent partitioning of radiant energy among surface heat fluxes was increasingly variable and is a result of the differing surface properties of the observation sites.

The results are broadly consistent with studies undertaken during the summertime in North American cities and suburbs, as well as European campaigns (Grimmond and Oke, 1995; 1999, Christen and Vogt, 2004, Offerle et al., 2006). The magnitude of Q^* was similar at both observation sites in unison with findings reported in Basel, Switzerland (Christen and Vogt, 2004). The urban fabric was a net energy store during the day time, the magnitude of which increased with increasing urban density. The proportioning of energy into heat storage was consistently greater during the day time at the urban location than its suburban counterpart. Fluxes of latent heat were greater at the suburban location which is expected for a location whose greenspace surface is greater in extent; however values for the summertime were still relatively low in comparison to other suburban EB studies where swimming pools and sprinkler systems were present (Grimmond and Oke, 1999). The relatively low magnitude of latent heat fluxes reported may also be as a result of the relative dryness of April and June in 2010. Precipitation recorded at Dublin Airport was 44 and 75% of baseline precipitation for April and June respectively. Furthermore no rainfall was recorded at least 7 days before the selected study days which would have affected the availability of water for evapotranspiration (Met Éireann).

Results reported here also confirm typical assumptions about the relative dryness and warmth of the urban atmosphere when compared to less dense suburban locations. Evaporation at the urban location is less than at the suburban location, as indicated by fluxes of latent heat. Sensible heat fluxes are almost always greater at the urban location, particularly

during all hour conditions. The release of heat from storage during the night time contributes to increases in fluxes of sensible heat. This phenomenon helped to give rise to the nocturnal UHI at the urban location during the observational campaign. At present unquantified advective influences mean that closure of the EB is difficult. The magnitude of storage heat flux, given that it is not a measured flux, presents the greatest uncertainty in the EB. This research employed the OHM to independently validate the EB residuals. Good agreement means that we can have confidence in our EB measured fluxes for the study campaign. That said however, the results reported here are preliminary and represent only two clear-sky, calm, twenty-four hour periods. Future research will require flux footprint modelling and analysis to ensure the spatial consistency of the EB during different meteorological conditions. The study days chosen for this particular study are not necessarily typical for Dublin so it will be necessary to investigate longer term datasets.

The anthropogenic heat flux, omitted for this study, warrants attention and would require data associated with transport use, space heating and cooling and population density. Furthermore instrumentation is in place for an in-depth evaluation of atmospheric carbon dioxide concentrations and fluxes, an increasingly popular and relevant area of urban climate science. A study of this kind would complement research in the area of urban EB studies and would create a more holistic picture of the urban effects on the urban and suburban atmosphere. In addition, observations being recorded at the two locations will prove important for initialising, parameterising and validating a future potential urban climate model for Dublin. The two observation locations were chosen for their widespread applicability. If we know the physical form of a neighbourhood and the associated urban climate response we can then begin to apply this knowledge to more widespread urban areas. In this way you can create a spatially disaggregated energy and emission flux database for urban areas in Dublin and Ireland.

Acknowledgements. The authors are very grateful to Dublin City Council, particularly the staff at Marrowbone Lane, and the staff and pupils of St. Pius X Girls National School for use of their buildings to site the instrumentation used in this study. The authors would like to acknowledge Ordnance Survey Ireland (Licence number EN 0063512) for providing the building footprints of the surrounds of the measurement sites. The authors would also like to acknowledge Met Éireann, the Irish meteorological service, for use of their data from Dublin Airport. The instrumentation was funded by the Higher Education Authority (HEA) and the authors gratefully acknowledge their input – this work would not have been possible without it. Finally, the authors would like to thank the anonymous reviewers for their helpful comments.

References

- Anandakumar, K. (1999) A study on the partition of net radiation into heat fluxes on a dry asphalt surface. *Atmospheric Environment*, 33(24–25), 3911–3918.
- Asaeda, T., Ca, V.T. and Wake, A. (1996) Heat storage of pavement and its effect on the lower atmosphere. *Atmospheric Environment*, 30(3), 413–427.
- Camuffo, D. and Bernardi, A. (1982) An observational study of heat fluxes and their relationships with net radiation. *Boundary Layer Meteorology*, 23, 359–368.
- Doll, D., Ching, J.K.S. and Kaneshiro, J. (1985) Parameterisation of subsurface heating for soil and concrete using net radiation data. *Boundary-Layer Meteorology*, 32, 351–372.
- Grimmond, C.S.B. and Oke, T.R. (1995) Comparison of heat fluxes from summertime observations in the suburbs of four North American cities. *Journal of Applied Meteorology* 34, 873–889.
- Grimmond, C.S.B. and Oke, T.R. (1999) Heat storage in urban areas: Local-scale observations and evaluation of a simple model. *Journal of Applied Meteorology*, 38, 922–940.
- Grimmond, C.S.B., Cleugh, H. and Oke, T.R. (1991) An objective urban heat storage model and its comparison with other schemes. *Atmospheric Environment. Part B. Urban Atmosphere*, 25(3), 311–326.
- Jauregui, E. and Luyando, E. (1999) Global radiation attenuation by air pollution and its effects on the thermal climate in Mexico City. *International Journal of Climatology* 19, 683–694.
- Met Éireann (2010) Rainfall. *Met Éireann Monthly Weather Bulletin*, Dublin, 288, April 2010, 1–16.
- Met Éireann (2010) Rainfall. *Met Éireann Monthly Weather Bulletin*, Dublin, 290, June 2010, 1–16.
- Narita, K.I., Sekine, T. and Tokuoka, T. (1984) Thermal properties of urban surface materials: study on heat balance at asphalt pavement. *Geographical Review Japan*, 57(Ser A), 639–651.
- National Centres for Environmental Prediction (2010) *Reanalysis Datasets at the Physical Sciences Division* [online]. Available at: <http://www.esrl.noaa.gov/psd/data/gridded/data.ncep.reanalysis2.surface.html> (accessed 1 June 2011).

- Offerle, B., Grimmond, C.S.B, Fortuniak, K. and Pawlak, W. (2006) Intraurban differences of surface energy fluxes in a central European city. *Journal of Applied Meteorology and Climatology* 45, 125–136.
- Oke, T.R. (2006) *Initial guidance to obtain representative observations at urban sites, Report No. 81*. Geneva: World Meteorological Organization.
- Oke, T.R. (1987) *Boundary Layer Climates* (2nd ed.) London: Routledge.
- Roberts, S.M., Oke, T.R., Grimmond, C.S.B. and Voogt, J. (2006) Comparison of four methods to estimate urban heat storage. *Journal of Applied Meteorology and Climatology*, 45(12), 1766–1781.
- Stanhill, J. and Kalma, J.D. (1995) Solar dimming and urban heating at Hong Kong *International Journal of Climatology*, 15(8), 933–941.
- Taesler, R. (1980) Studies of development and thermal structure of the urban boundary layer in Uppsala, Part I: Experimental Program; and Part II: Data analysis and results, Report 61. Uppsala: Meteorological Institute, Uppsala University.
- Yap, D.H. (1973) ‘Sensible heat fluxes in and near Vancouver, BC’. PhD Thesis, The University of British Columbia, Vancouver.
- Yoshida, A., Tominaga, K. and Watatani, S. (1990-91) Field measurements on energy balance of an urban canyon in the summer season. *Energy and Buildings*, 15–16, 417–423.